Available online at www.sciencedirect.com
ScienceDirect
Trans. Nonferrous Met. Soc. China 31(2021) 243−254
Transactions of Nonferrous Metals Society of China
www.tnmsc.cn

Preparation and properties of supersonic atmospheric plasma sprayed TiB_2−SiC coating

Ke ZOU[1,2], Jian-peng ZOU[1], Chun-ming DENG[2], Min LIU[2], Xue-zhang LIU[2], Rui-min ZHAO[3], Shun-hua LI[3], Ren-bo ZHU[1], Di GAO[1]

1. State Key Laboratory of Powder Metallurgy, Central South University, Changsha 410083, China;
2. Guangdong Key Laboratory of Modern Surface Engineering Technology, National Engineering Laboratory for Modern Materials Surface Engineering Technology, Guangdong Institute of New Materials, Guangzhou 510650, China;
3. Yunnan Yunlv Yongxin Aluminum Company Limited, Honghe 661400, China

Received 18 February 2020; accepted 28 October 2020

Abstract: With the TiB_2−SiC powders after spray granulation and vacuum calcination as raw materials, the TiB_2−SiC coating was prepared by supersonic atmospheric plasma spraying (SAPS). The effects of spraying power and spraying distance on the properties of the TiB_2−SiC coating were investigated and the fabrication processing of SAPS was optimized. The results show that the sprayed powders after calcination have a uniform particle size distribution, good sphericity and enhanced fluidity. The coating prepared by the calcined powders has a dense structure and high deposition efficiency. When the calcined TiB_2−SiC powders are used and the spraying power is 95 kW and the spraying distance is 150 mm during supersonic plasma spraying, the obtained TiB_2−SiC coating behaves the best comprehensive performance with the porosity, microhardness, bonding strength and resistivity equal to 5.6%, 3.57 GPa, 18.3 MPa and 10.8 mΩ·cm, respectively.

Key words: supersonic atmospheric plasma spraying (SAPS); TiB_2−SiC coating; vacuum calcination; processing optimization

1 Introduction

TiB_2 is an ideal inert wettable cathode material with high hardness, high melting point and good electrical conductivity. SiC has good chemical stability and high temperature stability, and its thermal expansion coefficient is 4.4×10^{-6} K^{-1}, which is less than 7.8×10^{-6} K^{-1} of TiB_2 and is closer to 2.0×10^{-6} K^{-1} of graphite. The addition of SiC to TiB_2 coating will produce small thermal mismatch and reduce the possibility of microcrack initiation, thus inhibiting the formation and propagation of cracks in the TiB_2-SiC coating on graphite substrate. At present, plasma spraying is mainly used to prepare coatings, and plasma spraying is a very complicated process, and each processing parameter will be affected by each other. Therefore, the spraying process parameters should be selected reasonably to achieve the coating with high bonding strength, good conductivity and high density [1,2]. TiB_2 coating has been served as a cathode material of aluminum electrolysis [3]. In the composite coating, the addition of SiC is very small, so the performance of the TiB_2−SiC coating is very close to that of the TiB_2 coating. Therefore, the TiB_2−SiC composite coating can be also served as the cathode material of aluminum electrolysis. It is necessary

Corresponding author: Jian-peng ZOU, Tel: +86-731-88876630, E-mail: zoujp@csu.edu.cn;
Chun-ming DENG, Tel: +86-20-61086656; E-mail: dengchunming@gdinm.com
DOI: 10.1016/S1003-6326(20)65491-7

to optimize the plasma spraying process to prepare TiB_2−SiC coating with an excellent performance to obtain a cathode material that can meet the requirements of aluminum electrolysis.

There are many parameters affecting the microstructure and properties of TiB_2−SiC coating, including the calcination of spray powders, the change of processing parameters and the choice of different spraying methods. The effects of spraying parameters on the coating properties have been studied [4−6]. The powders after spray granulation is agglomerated by the bonding action of the binder, and the bonding force between the particles is not strong and the pores among the particles are large. Therefore, the TiB_2−SiC powders need to be vacuum calcined to remove the organic binder. At the same time, the large particles are connected with the aggregated small particles [7−9], and the strength of the TiB_2−SiC agglomerated powders are increased. Plasma spray parameters have a large effect on particle velocity and particle temperature during fabricating the coating [10−12].

In this study, TiB_2−SiC powders were calcined at high temperatures, and a dense TiB_2−SiC coating was prepared by supersonic atmospheric plasma spraying (SAPS) with the calcined TiB_2−SiC powders. The processing parameters of supersonic plasma sprayed TiB_2−SiC coating were optimized, and the influence of the spraying power and the spraying distance on the performance of TiB_2−SiC coating was addressed especially.

2 Experimental

2.1 Vacuum calcination of TiB_2−SiC powders

The spray-granulated TiB_2−SiC powders were vacuum calcined according to the temperature rise curve of Fig. 1. The temperature was maintained at 300 and 500 °C for 2 h, respectively, to remove the organic binder among TiB_2−SiC particles [13]. The TiB_2−SiC large particles are bonded to small particles by calcination at a high temperature of 1400 °C for 2 h to increase the strength of the TiB_2−SiC powders. Thus, the calcined TiB_2−SiC powders have been obtained.

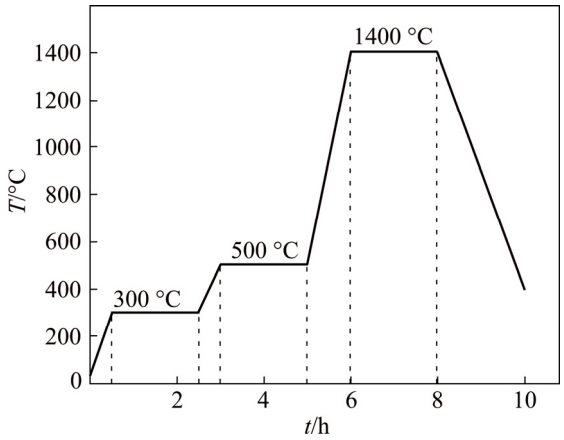

Fig. 1 Vacuum calcination curve of TiB_2−SiC powders

2.2 Supersonic plasma sprayed TiB_2−SiC coating

The 100HE supersonic plasma spraying system was used to spray the calcined and uncalcined TiB_2−SiC powders, respectively, and the effect of powder calcination on the properties of TiB_2−SiC coating was compared. The spraying parameters are shown in Table 1. Though there are many factors affecting the processing parameters in the plasma spraying process, the spraying power and the spraying distance are the most important parameters to control the performance of the coating. So this experiment mainly focused on these two parameters and studied their influence on the microstructure and properties of the TiB_2−SiC coating. The TiB_2−SiC coating numbers under different spraying parameters are shown in Table 2.

2.3 Performance characterization

The coating samples were cut with the Secotom-15 precision cutting machine, inlaid with CitoPress-5 semi-automatic inlay machine, and polished with the Tegramin-30 semi-automatic grinding and polishing machine. The morphologies of the powders and the coating were observed by Nova Nano SEM-430 (with EDS analysis) field emission scanning electron microscope (SEM). The phase structures of the powders and the coatings were analyzed by D8 advance X-ray diffractometer (Bruker, Germany). The K_α-ray of Cu target was

Table 1 Parameters of supersonic atmospheric plasma sprayed TiB_2−SiC coating

Spraying power/kW	Spraying distance/mm	Ar flow/ ($L\cdot min^{-1}$)	N_2 flow/ ($L\cdot min^{-1}$)	H_2 flow/ ($L\cdot min^{-1}$)	Carrier gas flow/($L\cdot min^{-1}$)	Powder feed rate/($g\cdot min^{-1}$)
95	150	40	28	34	11	14

Table 2 TiB_2−SiC coating numbers under different spraying parameters

Distance/mm	55 kW	75 kW	95 kW
120	1	2	3
150	4	5	6
180	7	8	9

used as diffracted source, the scanning step was 0.02 (°)/s, and the scanning range of 2θ was from 10° to 90°. Tensile method was used to measure the bonding strength of the TiB_2−SiC coating. The coating sample and the counterpart were bonded and fixed on the jig with adhesive, and the samples were kept in the oven at 180 °C for 3 h, and then the tensile test was carried out after cooling. The ratio of the fracture force to the cross-sectional area of the coating was the bonding strength of the coating. The hardness of the TiB_2−SiC coating samples was measured and characterized by MH−5D type Vickers microhardness tester, and the resistivity of the coating was measured by RTS−5 type double electric measurement four-probe tester. The microstructure of the coating was observed by Leica-Dmirm metallographic microscope. The porosity was measured by the proportion of local area pores in metallographic photos, which was calculated by Image-pro Plus software.

3 Results and discussion

3.1 Effect of powder calcination on morphology of TiB_2−SiC coating

The microscopic morphologies of the calcined TiB_2−SiC powders are shown in Fig. 2. It can be seen that the calcined TiB_2−SiC powders have a uniform particle size distribution and a dense microstructure. The uncalcined TiB_2−SiC powders have small particle size and uneven distribution, and contain many fine particles. The pores are large and the sphericity is not high, as shown in Figs. 2(a) and (c). The particle size of the calcined TiB_2−SiC powders is slightly larger than that of the uncalcined TiB_2−SiC powders, and the sphericity of the calcined TiB_2−SiC powders is obviously improved, the particles are evenly distributed, the

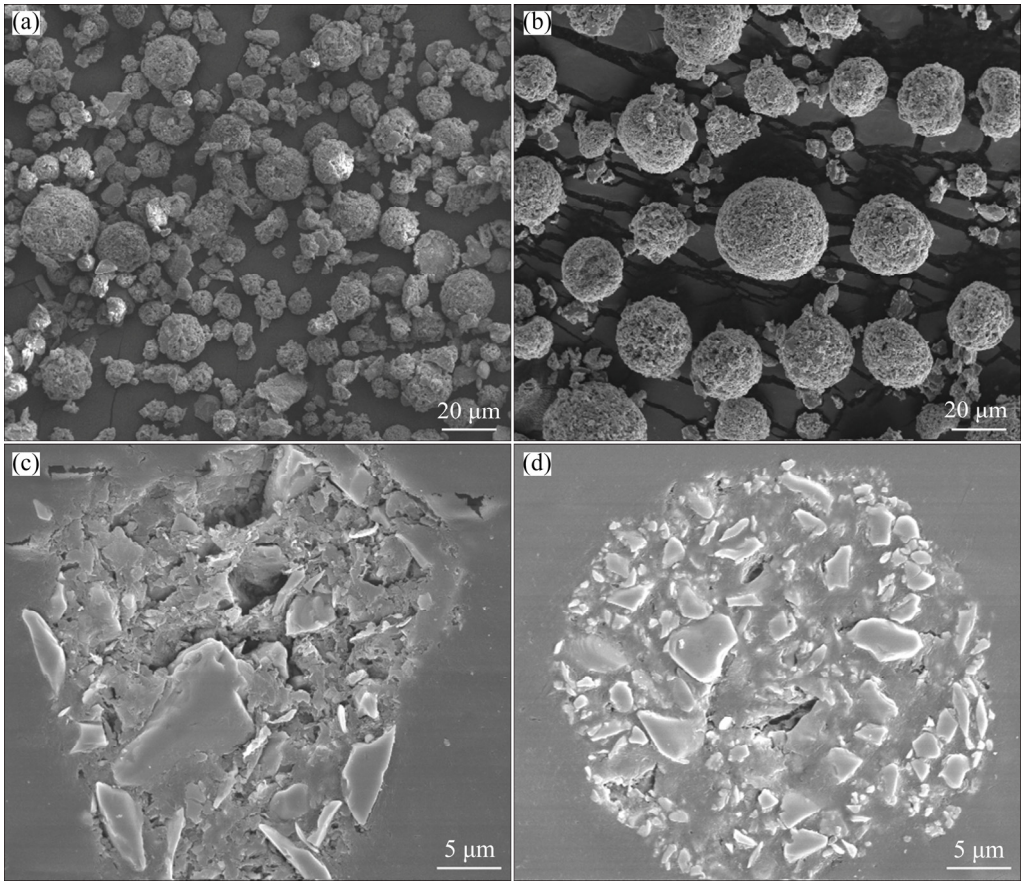

Fig. 2 Morphologies of uncalcined (a, c) and calcined (b, d) TiB_2−SiC powders: (a, b) Surface morphology; (c, d) Cross-sectional morphology

fluidity is enhanced, and the powder strength is improved, as shown in Figs. 2(b) and (d).

Referring to the spraying parameters in Table 1, the TiB_2−SiC coatings prepared by the calcined and uncalcined powders have been obtained, and their microscopic morphologies are shown in Fig. 3. It can be seen from Figs. 3(a) and (c) that the TiB_2−SiC coating prepared by the uncalcined powders has a loose structure, a large porosity, a certain degree of oxidation of the coating, and an oxide layer including TiO_2, B_2O_3 and SiO_2 distributed on the surface of the coating. It can be seen from Figs. 3(b) and (d) that the TiB_2−SiC coating prepared by the calcined powders has a dense structure, and the contents of the oxidized particles are decreased on the surface of coating and the oxidation phenomenon during the spraying process is obviously retarded. From Figs. 3(c) and (d), the thicknesses of the coating fabricated by uncalcined and calcined powders are 150 and 250 μm under the same spraying parameters, respectively, so the deposition efficiency of TiB_2−SiC coating prepared by calcined powders is obviously higher than that of TiB_2−SiC coating prepared by uncalcined powders.

3.2 Effect of powder calcination on performance of TiB_2−SiC coating

The phase structure and the EDS result of the TiB_2−SiC coatings are shown in Fig. 4. From the XRD analysis of Fig. 4(a), the main phase of TiB_2−SiC coating is TiB_2, and the TiB_2−SiC coating prepared by calcined powders has no obvious phase change with increase of the peak intensity and larger crystallinity of TiB_2−SiC phase compared with the uncalcined powders. The reason why the SiC phase cannot be detected may be that the SiC sublimation is caused by the temperature of the plasma flame current being too high during the plasma spraying process, so that the SiC content in the TiB_2−SiC coating is reduced, and the SiC phase cannot be detected. As shown in Fig. 4(b), it can be seen from EDS spectrum that TiB_2−SiC powder coating with calcined powders through plasma spraying is mainly composed of B, Ti, Si, C and

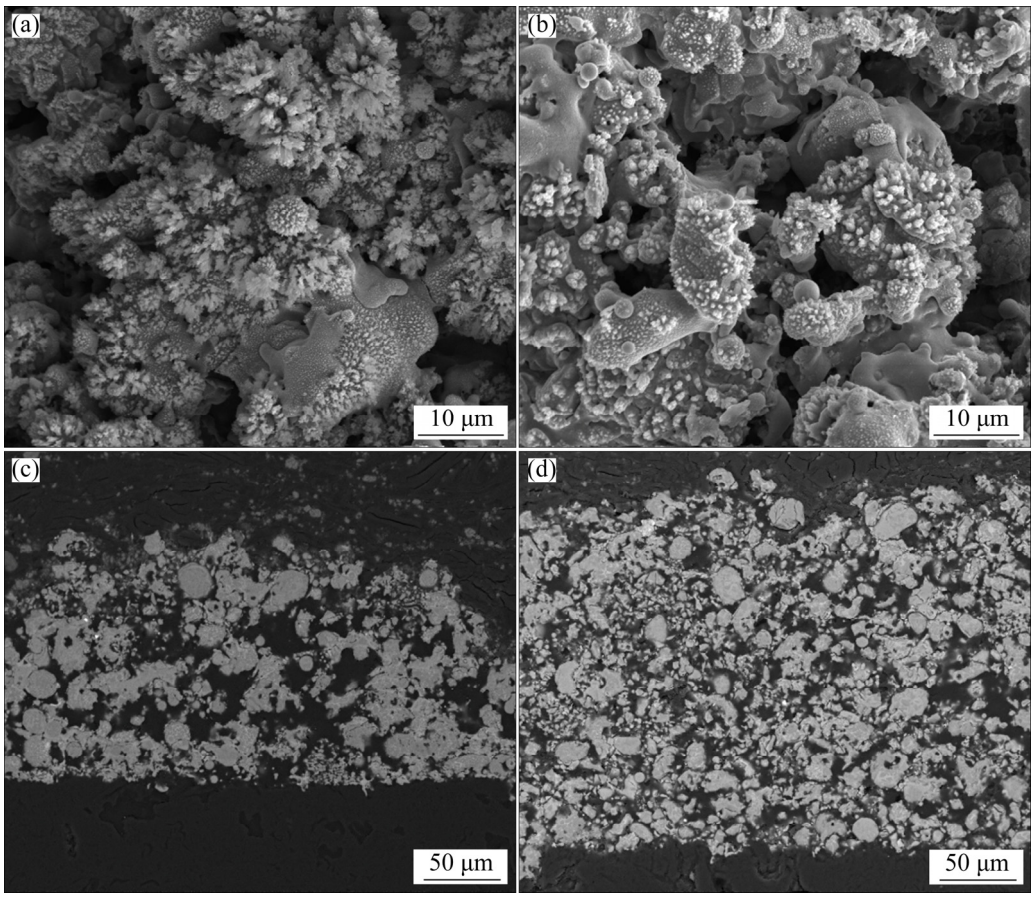

Fig. 3 SEM images of uncalcined (a, c) and calcined (b, d) TiB_2−SiC coatings prepared by SAPS: (a, b) Surface morphology; (c, d) Cross-sectional morphology

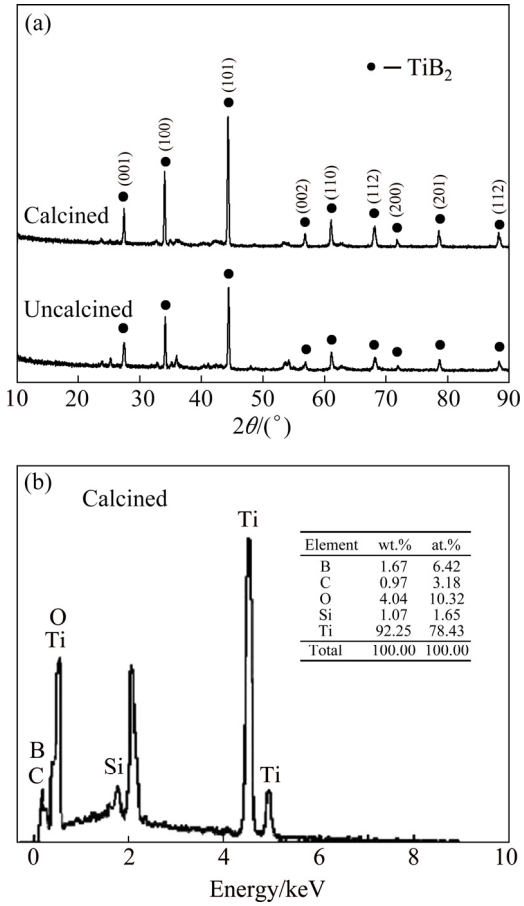

Fig. 4 XRD pattern (a) and EDS spectrum (b) of TiB_2−SiC coating

other elements, indicating that SiC still exists in the coating, although its content is too small to be detected in XRD.

The basic physical properties of the TiB_2−SiC coating prepared from the uncalcined powders and the calcined powders were characterized to further analyze the effect of powder calcination on the properties of TiB_2−SiC coating. The results are shown in Table 3. From the comparison of Table 3, the comprehensive performance of the TiB_2−SiC coating prepared by the calcined powders is significantly better than that of the TiB_2−SiC coating prepared by the uncalcined powders.

The porosity of the TiB_2−SiC coating prepared by calcined powders is significantly reduced. The reason is that the uncalcined TiB_2−SiC powders have a low strength and are easily broken in the plasma flame flow and cannot be stably heated in the center of the flame flow, so the particles are unevenly heated and pores are generated during spraying. The mechanical properties of the TiB_2−SiC coating prepared by calcined powders are also significantly improved. This is because the bonding force between the particles in the calcination process is changed from the binder adhesion to the connection between the large and the small particles. The bonding strength of the calcined powders is high, the coating obtained by spraying is uniform and compact, and the mechanical properties have been improved [14]. According to Table 3, the porosities of TiB_2−SiC coatings prepared from uncalcined and calcined powders are 11.3% and 5.6%, respectively. The former is much higher than the latter. The high porosity means high possibility of electron scattering during the process of electron transmission, which leads to a high resistivity. So the resistivity of TiB_2−SiC coating prepared by calcined powders is slightly lower than that of the coating prepared by the uncalcined powders.

In order to further study the effect of powder calcination on the mechanical properties of TiB_2−SiC coating, the morphology of TiB_2−SiC coating after tensile fracture was analyzed in Fig. 5. As shown in Fig. 5(a), many unmelted particles are distributed in the pores in the TiB_2−SiC coating prepared by the uncalcined powders, making it difficult to form a continuous molten TiB_2−SiC coating around the pores, resulting in stress concentration of the coating. The TiB_2−SiC coating prepared by calcined powders has a good melting morphology, consisting of molten particles and semi-molten particles, and the surface is flat and the coating is still dense, as shown in Fig. 5(b). It can be seen from the cross-sectional morphology that the pores are large and the cracks are generated in the TiB_2−SiC coating. Unmelted particles cannot merge into the coating totally. Abrupt transitional layer, rather than smooth transitional layer, appears

Table 3 Basic physical properties of TiB_2−SiC coating prepared from uncalcined and calcined powders

Coating	Porosity/%	Microhardness/GPa	Bond strength/MPa	Resistivity/(mΩ·cm)
Uncalcined	11.3	1.49	13.4	11.5
Calcined	5.6	3.57	18.3	10.8

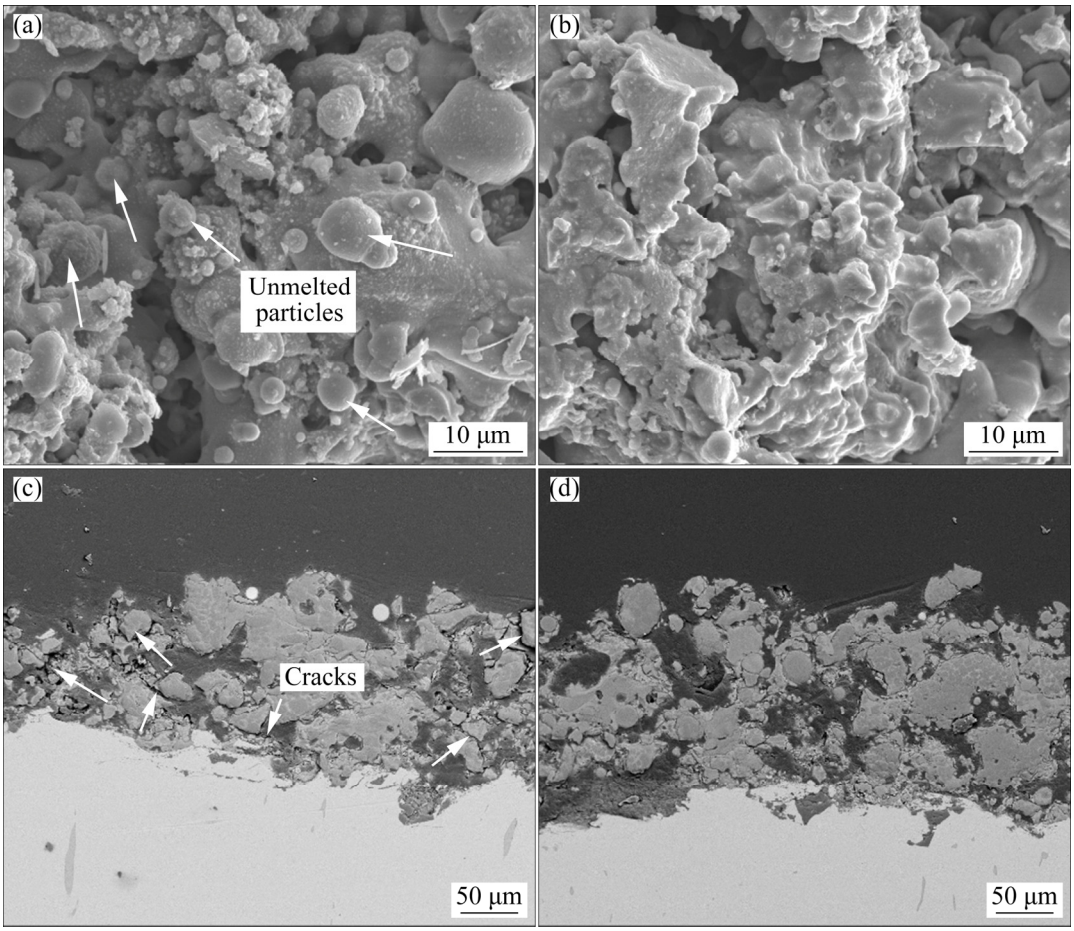

Fig. 5 SEM images of TiB_2−SiC coating prepared by uncalcined (a, c) and calcined (b, d) powders: (a, b) Surface morphology after stretching; (c, d) Post-stretched cross-section morphology

between the unmelted particles and the coating. Due to the sudden change of the transitional change, more unmelted particles will lead to more thermal coefficient mismatch in the coating and leads to a large thermal residual stress. Thus, the interface of the TiB_2−SiC coating prepared by the uncalcined powers has a large thermal residual stress due to more unmelted particles, and the cracks are formed at the joint between the inside of the coating and the coating/ substrate interface, as shown in Fig. 5(c). The TiB_2−SiC coating prepared by calcined powders has a dense interface without obvious cracking behavior. The bonding strength of the TiB_2−SiC coating prepared by the calcined powders is slightly higher than that of the TiB_2−SiC coating prepared by uncalcined powders, as shown in Fig. 5(d).

3.3 Effect of spraying process on microstructure of TiB_2−SiC coating

TiB_2−SiC coatings under different processing conditions were prepared, and the surface morphologies are shown in Fig. 6. It can be seen that the TiB_2−SiC coatings prepared under different processing conditions have different melting states and surface oxidation degrees.

The effect of the spraying power on the surface morphology of TiB_2−SiC coating is compared longitudinally in Fig. 6. It is found that when the spraying power is 55 kW, the coating melted poorly, and there are more unmelted and semi-molten particles, more pores without obvious oxidized particles on the surface, as shown in Figs. 6(a, d, g). When the spraying power is 75 kW, the melting effect of the coating is improved, but some semi-molten particles and unmelted particles are still generated, and the surface is slightly oxidized, as shown in Figs. 6(b, e, h). When the spraying power is 95 kW, the coating is in a molten state, consisting of molten particles and semi-molten particles, and more oxidized particles are generated on the surface, as shown in Figs. 6(c, f, i).

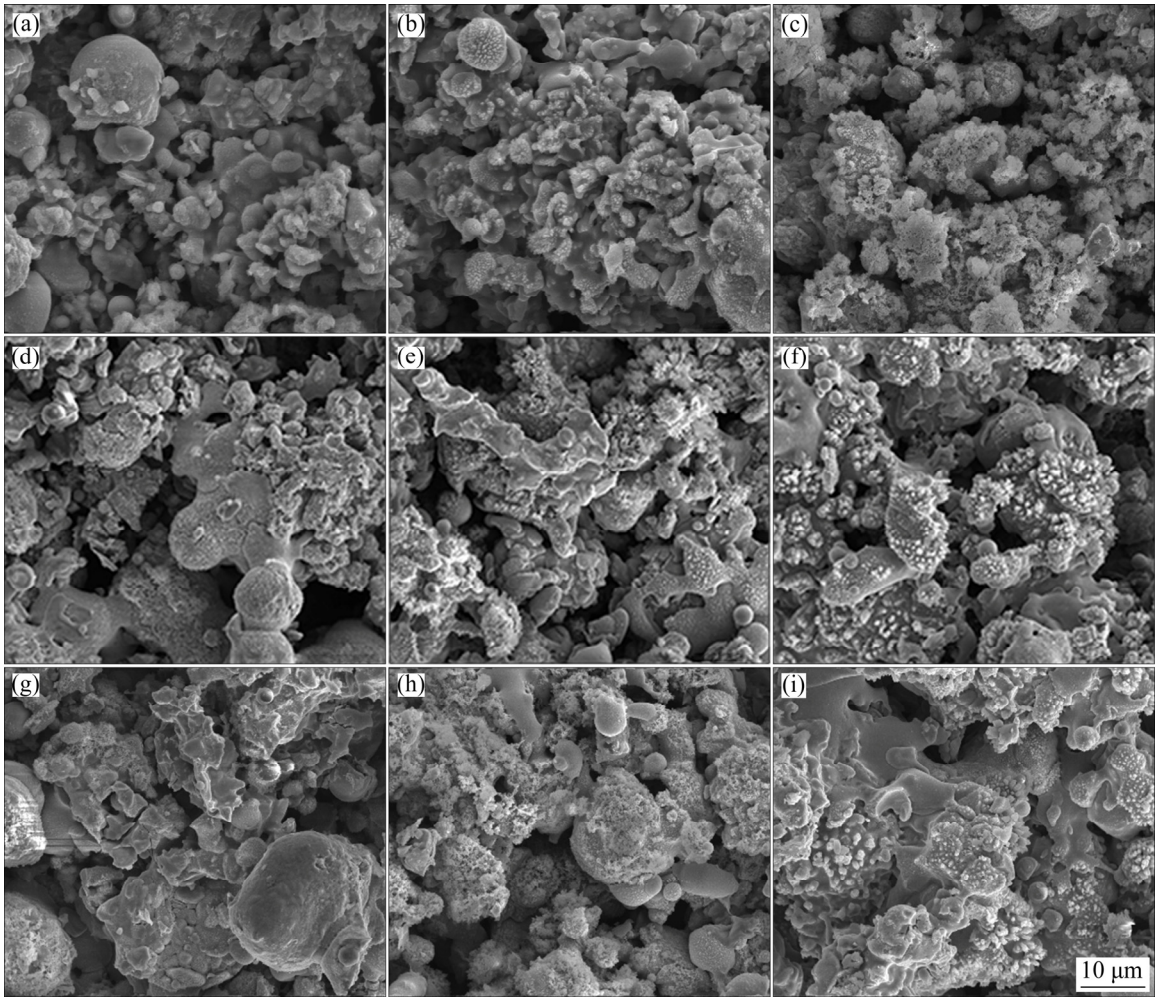

Fig. 6 Surface morphologies of TiB_2−SiC coating prepared under different processing conditions: (a) 120 mm, 55 kW; (b) 120 mm, 75 kW; (c) 120 mm, 95 kW; (d) 150 mm, 55 kW; (e) 150 mm, 75 kW; (f) 150 mm, 95 kW; (g) 180 mm, 55 kW; (h) 180 mm, 75 kW; (i) 180 mm, 95 kW

The effect of the spraying distance on the surface morphology of TiB_2−SiC coating is compared horizontally in Fig. 6. It is found that when the spraying distance is 120 mm, many particles with large particle size are not fully melted and the structure is loose, as shown in Figs. 6(a, b, c). When the spraying distance is 150 mm, the coating layer is in a molten state, which is formed by the stacking effect of molten and semi-molten particles, as shown in Figs. 6(d, e, f). When the spraying distance is 180 mm, the surface of the coating is fine and there are many large particles that are sufficiently melted, as shown in Figs. 6(g, h, i).

The cross-sectional morphologies of the TiB_2−SiC coating prepared under different processing conditions are shown in Fig. 7. It can be seen that the density and thickness of the TiB_2−SiC coating change with the processing conditions. Since the powder feeding rate, the spraying speed and the spraying time of the coating under different processes are the same, the deposition efficiency of the coating under different processes can be compared according to the thickness of the coating.

The effect of the spraying power on the cross-section morphology of TiB_2−SiC coating is compared longitudinally in Fig. 7. It is found that when the spraying power is 55 kW, the coating structure is loose, many pores are generated, the density is not high, and the deposition efficiency is low, as shown in Figs. 7(a, d, g). When the spraying power is 75 kW, the density of the coating is improved, the pores are reduced, the coating is dense, and the deposition efficiency is also high, as shown in Figs. 7(b, e, h). When the spraying power is 95 kW, the porosity of the layer is reduced and the density of the coating is significantly increased, as shown in Figs. 7(c, f, i).

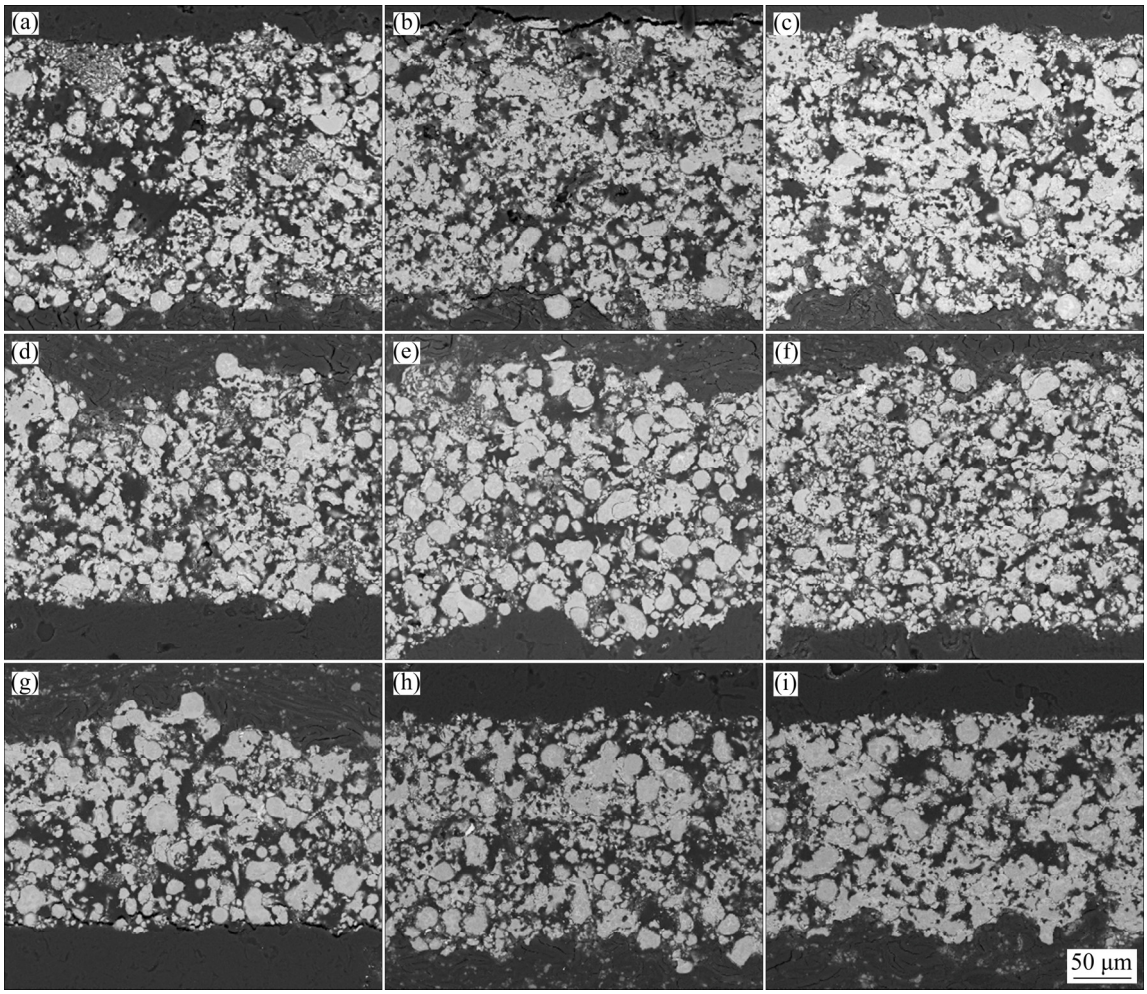

Fig. 7 Cross-sectional morphologies of TiB_2−SiC coating prepared under different processing conditions: (a) 120 mm, 55 kW; (b) 120 mm, 75 kW; (c) 120 mm, 95 kW; (d) 150 mm, 55 kW; (e) 150 mm, 75 kW; (f) 150 mm, 95 kW; (g) 180 mm, 55 kW; (h) 180 mm, 75 kW; (i) 180 mm, 95 kW

The effect of the spraying distance on the microstructure of TiB_2−SiC coating can be compared horizontally in Fig. 7. The porosity reflects the structure and the thickness reflects the deposition efficiency. It is found that when the spraying distance is 120 mm, the coating has many unmelted particles, the structure is loose, and the deposition efficiency is high, as shown in Figs. 7(a, b, c). When the spraying distance is 150 mm, the coating layer has a good molten state with compact structure and high deposition efficiency, as shown in Figs. 7(d, e, f). When the spraying distance is 180 mm, the thickness of the coating is relatively thin, the coating structure is loose and the deposition efficiency is low, as shown in Figs. 7(g, h, i).

The spraying power affects the temperature of the particles, which in turn affects the melting state of the particles [15]. When the spraying power is low, the TiB_2−SiC particles cannot be fully melted, so the porosity of the coating is high and the coating is not dense enough. When the spraying power is too high, the TiB_2−SiC particles with small particle size are easily to behave as super-melted state, which promotes the TiB_2−SiC coating to be oxidized on the surface. However, TiB_2 has a higher melting point and is more difficult to be melted. Therefore, it is necessary to appropriately increase the plasma spraying power to obtain the TiB_2−SiC coating with better comprehensive performance.

The spraying distance affects the flight time of the TiB_2−SiC particles in the plasma flame flow [16]. When the spraying distance is too short, the TiB_2−SiC particles are too late to be melted, the flying speed is small, and the particle impact deformation is insufficient. Thus the density and

bonding strength of the TiB_2−SiC coating can be decreased. When the spraying distance is too long, the molten TiB_2−SiC particles have not contacted with the substrate, the temperature and the flying speed begin to decrease, the bonding state of the TiB_2−SiC particles to the substrate is deteriorated, and the deposition efficiency is also lowered accordingly.

3.4 Effect of spraying process on properties of TiB_2−SiC coating

3.4.1 Porosity

Porosity is an important parameter to characterize the density of the coating. The porosity of the coating determines the corrosion resistance of the TiB_2−SiC coating [17]. If the coating porosity is too large, the molten salt electrolyte will penetrate into the cathode graphite matrix through the pores, reducing the bonding strength of the coating, resulting in cathode damage and shortening its service life.

Figure 8 shows the porosity changes of TiB_2−SiC coatings under different processing parameters. It can be seen that when the spraying distance is 120 mm, the porosity of the TiB_2−SiC coating is high. With the increase of the spraying distance, the porosity decreases to some extent. When the spraying power is 95 kW, the TiB_2−SiC coating is dense. The main reason is that when the spraying distance is too small, the residence time of the TiB2−SiC particles in the plasma flame flow is short, and they are not melted before reaching the substrate, so the formed coating structure is loose and the porosity is large. As the spraying distance increases, the TiB2−SiC particles remain in the plasma flame flow for a sufficient period of time to be fully melted, reaching the substrate to form a dense coating. In addition, the porosity decreases with the increase of the spraying power, which is consistent with the previous SEM analysis. Therefore, when the spraying distance is 150 mm and the spraying power is 95 kW, the porosity reaches the lowest value of 5.6%.

3.4.2 Microhardness

The use of a cathode coating in agitated aluminum fluid requires that the TiB_2−SiC coating should have certain microhardness to resist the scouring of the aluminum liquid.

Figure 9 shows the microhardness of TiB_2−SiC coatings under different processing parameters. It can be seen that the power has great influence on the microhardness of the TiB_2−SiC coating. When the spraying power is 95 kW, the microhardness of the TiB_2−SiC coating is obviously improved. This is mainly because TiB_2 has a higher melting point and requires a higher power to be fully melted, which makes the TiB_2−SiC coating structure denser, resulting in an increase in the microhardness of the TiB_2−SiC coating. Therefore, when the spraying distance is 150 mm and the spraying power is 95 kW, the microhardness of the obtained TiB_2−SiC coating reaches the highest value up to 3.57 GPa.

3.4.3 Bonding strength

The bonding strength of the coating is one of the important parameters for evaluating the quality of the coating. The higher the bonding strength, the better the quality of the coating and the longer the service life [18]. The bonding strength of the TiB2−SiC coating consists of two parts [19]: one is the cohesive force of the coated particles, and the

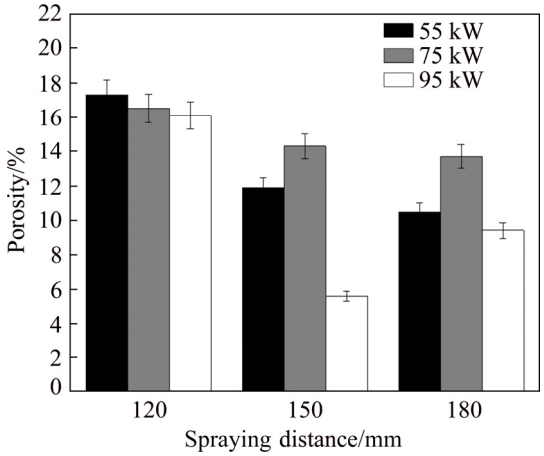

Fig. 8 Porosity of TiB_2−SiC coating prepared under different processing conditions

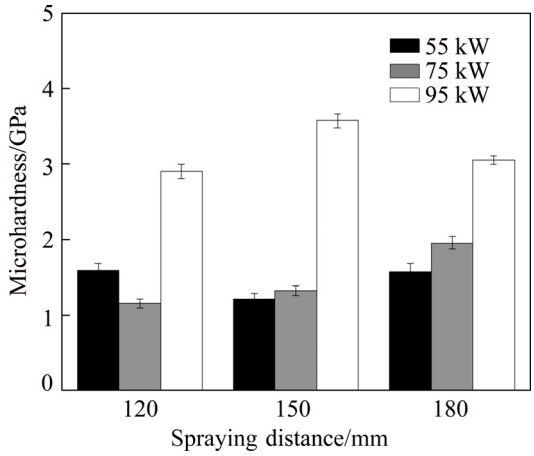

Fig. 9 Microhardness of TiB_2−SiC coating prepared under different processing conditions

other is the adhesion of the coating to the substrate. Usually, the cohesive force of the coating is greater than the interfacial adhesion between the coating and the substrate. Therefore, the bonding strength is decided by the interfacial adhesion. So only the interfacial bonding strength between the coating and the substrate is determined in this experiment.

Table 4 shows the interfacial bonding strength of TiB_2−SiC coatings with different spraying distances at a spraying power of 95 kW. The TiB_2−SiC coating has the highest bonding strength when the spraying distance is 150 mm. This is because when the spraying distance is small, the heating time of the TiB_2−SiC powders is short, the particle melting degree is insufficient, the coating structure is loose, and the bonding strength is lowered. When the spraying distance is too large, the flying speed of the TiB_2−SiC powders reaching the substrate is low, the powders cannot be sufficiently flattened, and the bonding strength of the coating is lowered.

Table 4 Bonding strength of TiB_2−SiC coating under different spraying distances

Spraying distance/mm	Bonding strength/MPa
120	10.5
150	18.3
180	15.2

Table 5 lists the interfacial bonding strength of the TiB_2−SiC coatings at different spraying powers with a spraying distance of 150 mm. It can be seen that as the spraying power increases, the bonding strength of the TiB_2−SiC coating increases to the highest value of 18.3 MPa. When the spraying power is too small, the TiB_2−SiC particles are not sufficiently melted since the melting point of the TiB_2−SiC powders is relatively high, resulting in more voids inside the coating and a decrease of bonding strength. At the same time, when the spraying power is too large, the TiB_2−SiC particles are super-melted, resulting in a low deposition efficiency of the TiB2−SiC coating and a decrease in bonding strength.

3.4.4 Conductivity

TiB_2−SiC coatings also need to have good electrical conductivity to reduce the cell voltage, improve current efficiency and increase the output of aluminum [20,21], so the conductivity of TiB_2−SiC coating is important for the TiB_2−SiC performance of the coating.

Table 5 Bonding strength of TiB_2−SiC coating under different spraying powers

Spraying power/kW	Bonding strength/MPa
55	11.3
75	15.6
95	18.3

Table 6 shows the resistivity of TiB_2−SiC coatings under different processing parameters. It can be seen that as the spraying power increases, the resistivity of the TiB_2−SiC coating gradually becomes smaller. When the spraying power is 95 kW, the resistivity is the smallest because the conductivity of the coating is affected by its density. When the spraying power is high, the TiB_2−SiC coating has better melting effect, higher density and better conductivity.

Table 6 Resistivity test results of TiB_2−SiC coating under different processing conditions

Spraying power/kW	Resistivity/(mΩ·cm)		
	120 mm	150 mm	180 mm
55	11.3	16.3	19.7
75	13.2	12.0	13.7
95	10.2	10.8	11.8

It can be concluded that when the TiB_2−SiC coating is prepared by calcined powders, the spraying power is 95 kW and the spraying distance is 150 mm, the comprehensive performance of the TiB_2−SiC coating is the best. These parameters are adopted by the subsequent TiB_2−SiC coating fabrication process.

4 Conclusions

(1) High-temperature vacuum calcination of TiB_2−SiC powders enhances the adhesion between particles, improves fluidity, and increases the strength of the powders. The porosity of TiB_2−SiC coating prepared by calcined powders is decreased, the microhardness and the bonding strength are increased, the electrical resistivity is decreased slightly, and the comprehensive performance is improved significantly.

(2) Spraying distance and spraying power have great influence on the microstructure and properties of the TiB_2−SiC coating. The spraying distance will affect the temperature and speed of the TiB_2−SiC particles in the plasma flame flow. The spraying power affects the molten state of the sprayed TiB_2−SiC powders during SAPS.

(3) The optimized processing parameters of the supersonic plasma sprayed TiB_2−SiC coating are calcined using TiB_2−SiC powders with a spraying distance of 150 mm and a spraying power of 95 kW. The TiB_2−SiC coating has the best overall performance of porosity of 5.6%, microhardness of 3.57 GPa, bonding strength of 18.3 MPa and resistivity of 10.8 mΩ·cm.

Acknowledgments

The authors are grateful for the financial supports from Guangdong Academy of Sciences Project (2018GDASCX-0402) of China, Yunnan Science and Technology Plan Project of China (2018IC080), and the Natural Science Foundation of Hunan Province of China (2018JJ2524).

References

[1] LV B W, XIE H, XU R, FAN X L, ZHANG W X, WANG T J. Effects of sintering and mixed oxide growth on the interface cracking of air-plasma-sprayed thermal barrier coating system at high temperature [J]. Applied Surface Science, 2016, 360: 461−469.

[2] DING X, CHENG X D, SHI J, LI C, YUAN C Q, DING Z X. Influence of WC size and HVOF process on erosion wear performance of WC−10Co−4Cr coatings[J]. International Journal of Advanced Manufacturing Technology, 2018, 96(8): 1615−1624.

[3] LI Q Y, LAI Y Q, LIU Y G, LI J, LIU Y X. Laboratory test and industrial application of an ambient temperature cured TiB_2 cathode coating for aluminum electrolysis cells [C]//Light Metals, 2004: 327−331.

[4] SU J B, ZHOU W C, WANG H Y, LIU Y, QING Y C, LUO F, ZHU D M, ZHOU L. Effect of critical plasma spray parameters on microstructure and microwave absorption property of Ti_3SiC_2/cordierite coatings [J]. Journal of Thermal Spray Technology, 2016, 25(4): 639−649.

[5] LI J, YANG G J, LI C J. Effect of vapor deposition in shrouded plasma spraying on morphology and wettability of the metallic Ni20Cr coating surface [J]. Journal of Alloys and Compounds, 2018, 735: 430−440.

[6] HOU G L, ZHAO X Q, AN Y L, ZHOU H D, CHEN J M. Effect of spraying parameter and injector angle on the properties of in-flight particles and alumina coatings on Al alloy with PA-HT [J]. Ceramics International, 2018, 44(3): 3173−3182.

[7] NI Z T, YANG X F, YANG X L, HE Q L, XU X W, XIE H H. Surface modification of ultrafine silicon nitride powders by calcination [J]. International Journal of Applied Ceramic Technology, 2019, 16(4): 1364−1372.

[8] VIANI A, SOTIRIADIS K, SASEK P, APPAVOU M S. Evolution of microstructure and performance in magnesium potassium phosphate ceramics: Role of sintering temperature of MgO powder [J]. Ceramics International, 2016, 42(14): 16310−16316.

[9] LV Y Q, FAN J L, HAN Y, LIU T. The influence of modification route on the properties of W−0.3wt%Y_2O_3 powder and alloy prepared by nano-in-situ composite method [J]. Journal of Alloys and Compounds, 2019, 774: 1140−1150.

[10] BOBZIN K, ÖTE M, SCHEIN J, ZIMMERMANN S. Numerical study on plasma jet and particle behavior in multi-arc plasma spraying [J]. Journal of Thermal Spray Technology, 2017, 26(5): 811−830.

[11] XING Y Z, LIU Z ,WANG G, LI X H, XING Y L, JIANG C P, CHEN Y N, SONG D X, DARGUSCH M. Effects of spray parameters on the adhesion between plasma-sprayed cast iron splat and aluminium substrate [J]. Surface and Coatings Technology, 2017, 315: 1−8.

[12] PUKASIEWICZ A G M, de BOER H E, SUCHARSKI G B, VAZ R F, PROCOPIAK L A J. The influence of HVOF spraying parameters on the microstructure, residual stress and cavitation resistance of FeMnCrSi coatings [J]. Surface and Coatings Technology, 2017, 327: 158−166.

[13] LEVASSEUR D, BROCHU M. Effect of heating rate on the pressureless sintering densification of a nickel-based superalloy [J]. Metallurgical and Materials Transactions A, 2016, 47(5): 2257−2266.

[14] GU S C, ZHU S Z, MA Z, HAN S P, LIU Y B. Preparation and properties of ZrB_2−$MoSi_2$-glass composite powders for plasma sprayed high temperature oxidation resistance coating on C/SiC composites [J]. Powder Technology, 2019, 345: 544−552.

[15] HOU G L, AN Y L, LIU G, ZHOU H D, CHEN J M, CHEN Z J. Effect of atmospheric plasma spraying power on microstructure and properties of WC−$(W,Cr)_2C$−Ni coatings [J]. Journal of Thermal Spray Technology, 2011, 20(6): 1150−1160.

[16] MOHAMMED S, MOTOHIRO Y, TOSHIAKI Y, MASAHIRO F. Synthesis of cubic aluminum nitride coating from Al_2O_3 powder in reactive plasma spray process [J]. Materials Transactions, 2013, 54(2): 207−214.

[17] WANG G, HUANG Z J, XIAO P, ZHU X B. Spraying of Fe-based amorphous coating with high corrosion resistance by HVAF [J]. Journal of Manufacturing Processes, 2016, 22: 34−38.

[18] TAN N, XING Z G, WANG X L, WANG H D, JIN G, XU B S. Investigation of sprayed particle filling qualities within the texture on the bonding behavior of Ni-based coating [J]. Surface and Coatings Technology, 2017, 330: 131−139.

[19] JENSEN M S, PEZZOTTA M, ZHANG Z L. Degradation of TiB_2 ceramics in liquid aluminum [J]. Journal of the European Ceramic Society, 2008, 28(16): 3155−3164.

[20] LIU Y, FU S H, WANG Z R, YAN X L, XI N Y, WU Y, CHEN H. Tensile properties, shear strength calculation and cracking behavior of bulk composite comprised of thick HVOF sprayed coating and steel substrate [J]. Surface and Coatings Technology, 2019, 374: 807−814.

[21] REN D L, DENG Q H, WANG J, YANG J S, LI Y B, SHAO J Q, LI M, ZHOU J, RAN S L, DU S Y, HUANG Q. Synthesis and properties of conductive B_4C ceramic composites with TiB_2 grain network [J]. Journal of the American Ceramic Society, 2019, 101(9): 3780−3786.

超音速大气等离子喷涂 TiB_2−SiC 涂层的制备与性能

邹 柯[1,2]，邹俭鹏[1]，邓春明[2]，刘 敏[2]，刘学璋[2]，赵瑞敏[3]，李顺华[3]，朱仁波[1]，高 迪[1]

1. 中南大学 粉末冶金国家重点实验室，长沙 410083；
2. 广东省新材料研究所 现代材料表面工程技术国家工程实验室
广东省现代表面工程技术重点实验室，广州 510650；
3. 云南云铝涌鑫铝业有限公司，红河 661400

摘 要：将喷雾造粒制备的 TiB_2−SiC 粉末进行真空煅烧，采用超音速大气等离子喷涂制备 TiB_2−SiC 涂层，研究喷涂功率和喷涂距离对 TiB_2−SiC 涂层性能的影响，并对超音速等离子喷涂制备 TiB_2−SiC 涂层的工艺进行优化。结果表明：煅烧后的喷涂粉末粒径分布均匀，球形度良好，流动性增强。煅烧粉末制备的涂层结构致密、沉积效率高。当采用超音速等离子喷涂煅烧后的 TiB_2−SiC 粉末、喷涂功率为 95 kW、喷涂距离为 150 mm 时，制备的 TiB_2−SiC 涂层综合性能最好：孔隙率为 5.6%，显微硬度为 3.57 GPa，结合强度为 18.3 MPa，电阻率为 10.8 mΩ·cm。

关键词：超音速大气等离子喷涂；TiB_2−SiC 涂层；真空煅烧；工艺优化

(Edited by Xiang-qun LI)